JGR Space Physics

RESEARCH ARTICLE
10.1029/2023JA031643

Extreme Geomagnetic Disturbances (GMDs) Observed in Eastern Arctic Canada: Occurrence Characteristics and Solar Cycle Dependence

Mark J. Engebretson[1], Lily Yang[1], Erik S. Steinmetz[1], Vyacheslav A. Pilipenko[2], Mark B. Moldwin[3], Brett A. McCuen[3], Martin G. Connors[4], James M. Weygand[5], Colin L. Waters[6], Yukitoshi Nishimura[7], Larry R. Lyons[8], and Christopher T. Russell[5]

[1]Department of Physics, Augsburg University, Minneapolis, MN, USA, [2]Space Research Institute, Moscow, Russia, [3]Department of Climate and Space Sciences and Engineering, University of Michigan, Ann Arbor, MI, USA, [4]Athabasca University Observatories, Athabasca University, Athabasca, AB, Canada, [5]UCLA Department of Earth Planetary and Space Sciences, Los Angeles, CA, USA, [6]University of Newcastle, Newcastle, NSW, Australia, [7]Department of Electrical and Computer Engineering and Center for Space Physics, Boston University, Boston, MA, USA, [8]Department of Atmospheric and Oceanic Sciences, University of California, Los Angeles, Los Angeles, CA, USA

Key Points:

- Most large (6 nT/s) and extreme (>20 nT/s) high latitude geomagnetic disturbances (GMDs) occurred during the declining phase of the sunspot cycle
- Most extreme GMDs occurred during high-speed solar wind streams and often within 25 min after a substorm onset, but seldom within 5 min
- Many extreme GMDs showed a poleward progression, consistent with the tailward retreat of the magnetotail reconnection region

Correspondence to:
M. J. Engebretson,
engebret@augsburg.edu

Citation:
Engebretson, M. J., Yang, L., Steinmetz, E. S., Pilipenko, V. A., Moldwin, M. B., McCuen, B. A., et al. (2024). Extreme geomagnetic disturbances (GMDs) observed in Eastern Arctic Canada: Occurrence characteristics and solar cycle dependence. *Journal of Geophysical Research: Space Physics*, *129*, e2023JA031643. https://doi.org/10.1029/2023JA031643

Received 25 APR 2023
Accepted 1 DEC 2023

Author Contributions:
Conceptualization: Mark J. Engebretson
Data curation: Erik S. Steinmetz, Brett A. McCuen, Martin G. Connors
Formal analysis: Mark J. Engebretson
Funding acquisition: Mark J. Engebretson
Investigation: Mark J. Engebretson, Lily Yang, Vyacheslav A. Pilipenko, Mark B. Moldwin, Brett A. McCuen, Martin G. Connors, James M. Weygand, Colin L. Waters, Yukitoshi Nishimura, Larry R. Lyons, Christopher T. Russell
Methodology: Mark J. Engebretson, James M. Weygand

Abstract Extreme (>20 nT/s) geomagnetic disturbances (GMDs, also denoted as MPEs—magnetic perturbation events)—impulsive nighttime disturbances with time scale ~5–10 min, have sufficient amplitude to cause bursts of geomagnetically induced currents (GICs) that can damage technical infrastructure. In this study, we present occurrence statistics for extreme GMD events from five stations in the MACCS and AUTUMNX magnetometer arrays in Arctic Canada at magnetic latitudes ranging from 65° to 75°. We report all large (≥6 nT/s) and extreme GMDs from these stations from 2011 through 2022 to analyze variations of GMD activity over a full solar cycle and compare them to those found in three earlier studies. GMD activity between 2011 and 2022 did not closely follow the sunspot cycle, but instead was lowest during its rising phase and maximum (2011–2014) and highest during the early declining phase (2015–2017). Most of these GMDs, especially the most extreme, were associated with high-speed solar wind streams (Vsw >600 km/s) and steady solar wind pressure. All extreme GMDs occurred within 80 min after substorm onsets, but few within 5 min. Multistation data often revealed a poleward progression of GMDs, consistent with a tailward retreat of the magnetotail reconnection region. These observations indicate that extreme GIC hazard conditions can occur for a variety of solar wind drivers and geomagnetic conditions, not only for fast-coronal mass ejection driven storms.

Plain Language Summary Geomagnetically induced currents (GICs) can give rise to the most extreme space weather impact of disrupting electric power distribution. GICs can be driven by extreme geomagnetic disturbances (GMDs) that are observed as large amplitude (several hundred nT amplitude) and rapid (5–10 min period) changes in the geomagnetic field. We found that extreme high-latitude GMDs occur throughout the solar cycle, but are preferentially observed during the declining phase of the solar cycle (the several year interval just past solar maximum) and in conjunction with high-speed solar wind streams. They also all occur within 80 min of a geomagnetic substorm, but are not directly related to its explosive onset. These GMDs are most often observed to propagate poleward consistent with tailward retreat of magnetotail reconnection regions. These results show that extreme GMDs and hence large GICs can be driven by a variety of solar wind conditions and not just fast coronal mass ejections.

1. Introduction

Large nighttime geomagnetic disturbances (GMDs) are known as magnetic perturbation events (MPEs) which are perturbations of 5–10 min duration and amplitudes of hundreds or more nT. These perturbation events are known to be causally related to geomagnetically induced currents (GICs) that can flow in long conductors such as electrical power lines, pipelines, and undersea cables (Boteler et al., 1998; Gannon et al., 2019; Ngwira & Pulkkinen, 2019). GICs are one of several phenomena included in the field of space weather that are triggered by increased solar activity that lead to dangerous levels of magnetospheric and ionospheric disturbances. Extreme GIC events that extend to middle and even low latitudes have been identified for over a century, beginning with the "Carrington event" in 1859 (Carrington, 1859; Cliver & Dietrich, 2013; Tsurutani et al., 2003) and include

those related to large geomagnetic storms in May 1921 and March 1989 (Boteler, 2019; Hapgood, 2019; Love et al., 2019). Early reviews focused on the generation of GICs during geomagnetic storms (e.g., Kappenman, 2005), but more recent studies have found that large nighttime GMDs are often more closely related to substorms, which can occur during both storm and non-storm times.

Great (low-latitude) aurorae and related extreme GIC events are associated chiefly with coronal mass ejection (CME)-driven storms and rarely with corotating interaction region (CIR)-driven storms because the aurorae do not progress as far equatorward for CIR-driven storms (Borovsky & Denton, 2006). Borovsky and Denton (2006) also noted that both CIRs and the high-speed solar wind streams (HSS) that typically follow them can be drivers of storms, and that when recurring CIR-driven storms were ongoing (which tends to be in the declining phase of the solar cycle), the durations of high-speed streams were longer. Mursula et al. (2022) showed the importance of variations in the width of the heliospheric current sheet (HCS) for the relative occurrence of geomagnetic storms related to CMEs, HSS/CIRs, and slow solar wind, respectively, such that a wide HCS made large and moderate HSS/CIR storms occur in the early declining phase in recent cycles 23 and 24 (1996–2019), while in the more active cycles 20–22 (1964–1996) they occurred in the late declining phase (their Figure 5).

Tsurutani et al. (2006) reviewed the causes, characteristics, and consequences of CIRs and high-speed streams, in particular their association with auroral substorms. Tsurutani and Gonzalez (1987) denoted the high-speed stream following the passage of a CIR past Earth as a High Intensity Long Duration Continuous AE Activity (HILDCAA) interval. HILDCAAs were originally identified during solar maximum years as intervals during which the AE index remained above 200 nT for 48 hr and that AE < 200-nT intervals were less than 2 hr in duration. However, Tsurutani et al. (1995) noted that similar extended intervals observed during the declining phase of the sunspot cycle were characterized by continuous auroral substorms stimulated by large-amplitude Alfvén waves within the high-speed streams. Tsurutani et al. (2011) concluded that the major cause of geomagnetic activity during high-speed streams is large amplitude interplanetary Alfvén waves.

There have been significant efforts worldwide to understand and forecast GICs, by developing empirical and numerical models that can predict their timing and locations (Morley, 2020). Considerable success has been achieved for predicting large-scale magnetospheric features but predicting dB/dt events with amplitude larger than 1.5 nT/s remains a challenge (Pulkkinen et al., 2013, 2017). Morley (2020) noted that while coupled frameworks and global MHD models have been shown to perform well (on average) at predicting the Dst index (Liemohn et al., 2018) and have had some success at predicting geomagnetic perturbations (Pulkkinen et al., 2013), statistical studies of simulations have shown a significant tendency to underestimate the magnitude of auroral zone magnetic perturbations (Haiducek et al., 2017; Pulkkinen et al., 2013).

More recently, Al Shidi et al. (2022) noted the Space Weather Modeling Framework (SWMF)Geospace model used by the NOAA Space Weather Prediction Center (SWPC) to produce ground magnetic perturbation maps has been comprehensively validated with respect to predictions of Dst and the polar cap potential (Pulkkinen et al., 2022). The Al Shidi et al. (2022) results showed that regional predictions at mid-latitudes were quite accurate, but that high-latitude regional disturbances were difficult to predict. Pilipenko et al. (2023) also tested this model, found that the predicted magnetic field variability dB/dt in East Scandinavia was more than an order of magnitude less than that observed, and suggested that there might be some magnetotail physics that is not captured in current global models.

Al Shidi et al. (2022) noted that the difficulty in predicting high-latitude regional disturbances reflects the tendency of this model to miss strong auroral zone latitude activity associated with substorms or other localized magnetotail processes that drive currents that couple to the ionosphere. Juusola et al. (2023) noted that Pulkkinen et al. (2003) and more recently Dimmock et al. (2019) have suggested that GICs are primarily driven by small-scale spatiotemporal structures superimposed on the large-scale westward electrojet (WEJ). Weygand et al. (2021) confirmed this using a large statistical study finding that most nighttime GMDs occurred under a westward electrojet, including many within the Harang current system, the three-region pattern of field-aligned current flow in the Harang discontinuity region that according to the early study of Iijima and Potemra (1978) is highly variable and develops complicated features throughout intervals of substorm activity. Several studies have shown that nighttime GMDs were highly localized, with half-amplitude radii of a few hundred km (Ngwira et al., 2018; Engebretson et al., 2019a, 2019b; Dimmock et al., 2020; Weygand et al., 2021).

Kwagala et al. (2020) found that the version of the SWMF model they used predicted the occurrence of low derivative threshold (0.3 nT/s) intervals in a set of stations in northern Europe at a rate very close to the frequency

Table 1
Locations of the Magnetometer Stations Used in This Study

Array	Station	Code	Geog.Lat	Geog.Lon	CGM.Lat.	CGM.Lon.	UT of mag midnight
MACCS	Repulse Bay	RBY	66.5°	273.8°	75.2°	−12.8°	05:47
	Cape Dorset	CDR	64.2°	283.4°	72.7°	3.0°	04:58
	Pangnirtung	PGG	66.1°	294.2°	73.3°	19.8°	03:53
AUTUMNX	Salluit	SALU	62.2°	284.3°	70.7°	4.1°	04:54
	Kuujjuarapik	KJPK	55.3°	282.2°	64.7°	0.2°	05.06
Interstation Distances:		RBY-CDR		512 km			
		CDR-PGG		546 km			
		CDR-SALU		226 km			
		SALU-KJPK		776 km			

Note. Geographic and corrected geomagnetic (CGM) latitude and longitude are shown, as well as the universal time (UT) of local magnetic midnight. Distances between nearest-neighbor pairs of stations are also presented. CGM coordinates were calculated for epoch 2015, using http://sdnet.thayer.dartmouth.edu/aacgm/aacgm_calc.php#AACGM.

of occurrence in reality, but that as the threshold was increased to 1.1 and 1.5 nT/s the model diverged from the real-world rate, under-estimating at lower latitudes and sometimes overestimating at higher magnetic latitudes. The model mostly underestimated the large amplitude short-lived perturbations likely associated with localized current structures. We note that it is precisely these large amplitude, localized events that comprise a large portion of ≥6 nT/s nighttime GMDs.

Our earlier studies of ≥6 nT/s nighttime GMDs using data from Arctic Canada (Engebretson et al., 2019a, 2019b, 2021a, 2019b) covered only two years (2015 and 2017) and focused on latitude- and local time-dependent occurrence patterns and short-term dependencies on solar wind/IMF parameters and magnetospheric activity indices. This study documents the occurrence of these largest GMDs at auroral latitudes over a nearly complete solar cycle and shows their frequent association with high speed solar wind streams and conditions following substorm onsets. Section 2 describes the data set and analysis methods used to identify events. Section 3 compares the solar cycle distributions of ≥6 nT/s GMD events, sunspots, solar wind velocity, and substorm onsets. Section 4 presents an analysis of extreme (>20 nT/s) GMDs and their relation to other physical quantities and indices. Section 5 presents similarities observed in three earlier studies of multiyear GMD data sets. Section 6 discusses some of the implications of these observations, and Section 7 summarizes the findings.

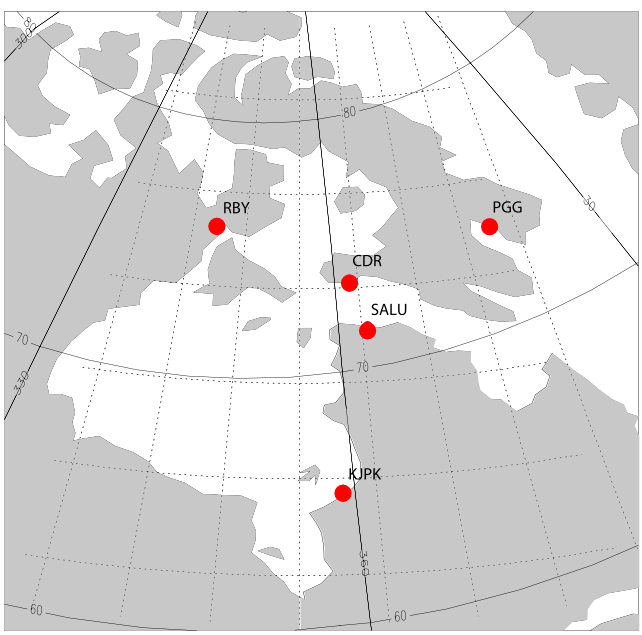

Figure 1. Map of ground magnetometer stations used for this study. Selected latitude and longitude lines in geomagnetic coordinates are shown.

2. Magnetometer Data Set

Vector magnetometer data used in this multi-year study were recorded at five stations in the MACCS (Engebretson et al., 1995, 2011) and AUTUMNX (Connors et al., 2016; Reiter et al., 2021) arrays in Eastern Arctic Canada with corrected geomagnetic latitude (MLAT) ranging from 64.7° to 75.2°, all within 20° of the 0° magnetic meridian, as detailed in Table 1 and Figure 1. The Magnetometer Array for Cusp and Cleft Studies (MACCS) began operation in 1992, and the Athabasca University Themis UCLA Magnetometer Network-Extended (AUTUMNX) began operation in late 2014. Data from both arrays were sampled at a 2 Hz cadence and are presented in local magnetic coordinates with sensor axes oriented as follows: X: magnetic north, Y: magnetic east, and Z: vertically down. Events during 2015 and 2017 from these and other neighboring stations in Arctic Canada have been used in several recent studies by Engebretson et al. (2019a, 2019b, 2021a, 2021b) and Weygand et al. (2021).

All available daily data files obtained from January 2011 through December 2022 (covering approximately one solar sunspot cycle) from each of the

Table 2
Number of Available Station Days, ≥6 and >20 nT/s GMD Events, and Percent of GMDs per Station Day Observed From 2011 Through 2022

Year	2011	2012	2013	2014	2015	2016	2017	2018	2019	2020	2021	2022
Station days	452	587	767	1213	1682	1346	1542	1677	1520	1377	1328	1672
≥6 nT/s GMDs	69	82	88	131	611	550	745	460	398	289	330	528
% ≥6 nT/s	15.3	14.0	11.5	10.8	36.3	40.9	48.3	27.4	26.2	21.0	24.9	31.6
>20 n/s GMDs	0	2	3	0	14	11	18	6	5	1	3	9
% >20 nT/s	0	0.34	0.39	0	0.83	0.82	1.17	0.36	0.33	0.07	0.23	0.54

three MACCS stations (RBY, PGG, and CDR) and two AUTUMNX stations (SALU, KJPK) were analyzed to identify GMDs with ≥6 nT/s amplitude. GMD amplitude thresholds of 1 nT/s have been used in many studies (e.g., Viljanen et al., 2001) and more recently by Juusola et al. (2023). A higher threshold level for GIC hazards of 5 nT/s was identified by Molinski et al. (2000), Boteler (2001), and Woodroffe et al. (2016), so the ≥6 nT/s events identified in this study would pose significant threats to electrical infrastructure if any were present near these sites. The GMDs in the >20 nT/s subset are comparable in amplitude to those measured during extreme GIC events at lower latitudes. Nine of them exceeded 30 nT/s, and the two largest, on 15 March 2012 and 15 September 2017, had values of 44.1 and 43.3 nT/s, comparable to the largest value cited by Mac Manus et al. (2022) of ∼2700 nT/min = ∼45 nT/s recorded at the Lovo observatory (55.8° CGM latitude) near Stockholm, Sweden in July 1982 (Kappenman, 2006). We remind readers, however, that large GMDs only constitute the first (but essential) step in producing GICs that pose a threat to electrical infrastructure. The spatial arrangement and value of the underlying ground conductivity, the presence of extended conducting structures (power lines and pipelines) and their orientation relative to the driving auroral currents, and the orientation and ground connections of power grid structures such as transformers all play a role in determining the severity of the resulting GICs (Arajärvi et al., 2011; Boteler & Pirjola, 2017; Viljanen et al., 2013).

Event identification made use of a semi-automated process described in detail in Engebretson et al. (2019a). This procedure began by displaying a daily magnetogram (a 24-hr 3-axis plot of the magnetic field at a given station) on a computer screen. Once a rapid (<20 min duration) and large amplitude (>∼200 nT) magnetic perturbation along any axis was visually identified, the IDL cursor function was used to select times ∼15–60 min before and after the perturbation to zoom in on the relatively short duration of the event and separate it from the times of other possible activity. After application of a 10-point boxcar mean smoothing to reduce noise and eliminate isolated non-physical spikes, the data were numerically differentiated using the 3-point Lagrangian approximation. The times and values of extrema of B and dB/dt for all three components in this interval were recorded for completeness, as also did Milan et al. (2023), and plots of the time series of data and derivatives were produced and saved. If more than one interval with a ≥6 nT/s derivative in one or more components was identified on a given day, this process was repeated as necessary. The minimum length of each interval was chosen to be ∼5 min, so multiple peak derivatives ≥6 nT/s occurring within a given ∼5 min interval were not counted separately. A subset of 72 events with a >20 nT/s derivative in one or more components was identified from this data set.

3. Yearly Distribution of ≥6 nT/s GMDs, Sunspots, Solar Wind Velocity, and Substorm Onsets

Table 2 summarizes the data set used in this study. Although the magnetometer and recording instrumentation at all MACCS stations were set up to record continuously from 2011 through 2022, and at all AUTUMNX stations from late 2013 through 2022, power outages, cut cables, and instrument malfunctions at these remote sites often resulted in no data or erroneous data at individual stations. We thus show in this table the number of available valid station days per year and the total number of ≥6 and >20 nT/s GMD events and the percent ratio of these events per available station day.

Figure 2a shows the occurrence percentages of ≥6 nT/s GMDs from each of the five stations from 2011 through 2022. Note that the traces for AUTUMNX stations SALU and KJPK began in 2014, and there were no data from SALU during 2020 or from RBY during 2011. The overall trend at each station is similar, and from 2016 through 2022 there is a clear pattern in magnetic latitude. Percentages are smallest at the highest MLAT station, RBY, and

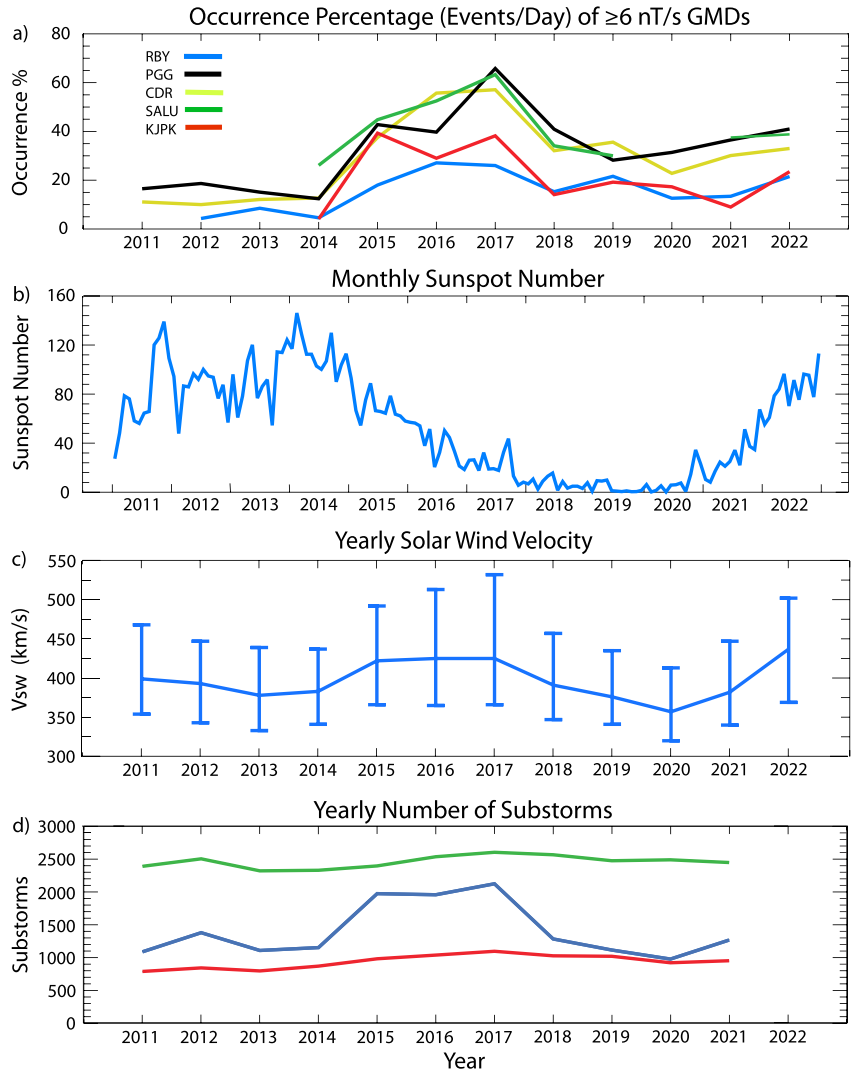

Figure 2. (a) Yearly occurrence percentages (events/station day) of ≥6 nT/s GMDs observed at five sites in Eastern Arctic Canada from 2011 through 2022. (b) Monthly sunspot numbers from January 2011 through December 2022. (c) Yearly medians and 25th and 75th percentile values (lower and upper bars) of the solar wind velocity and (d) Yearly number of substorm onsets from 2011 through 2021 identified in the three substorm lists provided by SuperMAG: green (Forsyth et al., 2015), blue (Newell & Gjerloev, 2011), and red (Ohtani and Gjerloev, (2020).

at the lowest MLAT station, KJPK, and are larger and generally similar at the three stations at latitudes between these extremes. We note that the occurrence rates shown in Table 2 (percent of GMDs per station day during each year) are averages over all five stations, so they fall between the extremes shown in Figure 2a for individual stations.

Figure 2b shows the monthly sunspot numbers, obtained from the Solar Influences Data Center (https://sidc.be/silso/datafiles/), from January 2011 through December 2022. The rising phase and maximum of sunspot cycle 24 (2011–2014) coincided with low occurrence percentages of GMDs, whereas the declining phase (2015–2017) coincided with high GMD occurrence percentages. The late declining phase and sunspot minimum (2018–2020) coincided again with decreasing GMD occurrence percentages. The early rising phase of Cycle 25 coincided with rising GMD occurrence percentages; GMD occurrence percentages in 2022 were considerably larger than those 11 years earlier (2011) at the same stations, PGG and CDR.

Figure 2c shows yearly medians and 25th and 75th percentile values of the solar wind velocity (Vsw), based on 1-hr averages obtained from the OMNI database via CDAWEB (https://cdaweb.gsfc.nasa.gov/) for these same years. The largest annual median and especially 75th percentile velocities coincided in time with the largest GMD

occurrence percentages (2015–2017) and the smallest annual velocities (2013–2014 and 2020) coincided approximately with the smallest GMD occurrence percentages (2012–2014 and 2020). The fractional range in GMD occurrences (a factor of ∼3) was much larger than the fractional range of Vsw values. We note especially that the 75th percentile values were further from the median than the 25th percentile values during 2015–2017 and 2019, indicating a more extended high-velocity tail of the Vsw distributions during those years.

Figure 2d shows the yearly number of substorm onsets from 2011 through 2021 identified in three substorm lists provided at the SuperMAG web site (https://supermag.jhuapl.edu/substorms/): Newell and Gjerloev (2011), Forsyth et al. (2015), and Ohtani and Gjerloev (2020), each of which used a different set of criteria to identify onsets based on values of the SuperMAG SML index (https://supermag.jhuapl.edu/indices). (Note that as of 11 October 2023 no substorm lists were available for year 2022.) Forsyth et al. identified onsets on the basis of exceedance of a percentile in the rate of change of SML. The Newell and Gjerloev and Ohtani and Gjerloev (2020) criteria required sharp and sustained drops in SML which differed primarily in that the Ohtani and Gjerloev criteria identified only isolated substorms. In several of our recent papers we have found that a significant fraction of events within 1–2 hr of ≥6 nT/s GMDs were listed mutually exclusively in the Forsyth et al. and Newell and Gjerloev lists, and many of these did not appear in the Ohtani and Gjerloev list.

The three traces in Figure 2d are similar to each other and to the traces in Figures 2a and 2c in showing a solar cycle dependence with a peak during the declining phase, but the three traces in Figure 2d show significant differences in both the numbers of onsets and the degree of their enhancement during 2015–2017. The ratios of maximum to minimum values in these panels are ∼5 for GMD occurrences in Figure 2a, 1.2 for mean Vsw in Figure 2c, and 1.1, 2.2, and 1.4 for the green, blue, and red substorm number traces in Figure 2d.

The exclusion of closely-spaced substorm onsets in the red trace in Figure 2d, based on the Ohtani and Gjerloev (2020) criteria, may explain the smaller maximum in yearly onsets during 2015–2017 compared to the blue trace, because during the declining phase of the solar cycle a greater number of HILDCAA intervals are expected to occur (Tsurutani et al., 1995), making identification of onsets during such "High Intensity Long Duration Continuous AE Activity" intervals more difficult. We can only speculate that the lower ratios in the green and red traces in Figure 2d may suggest a tendency in both the Forsyth et al. (2015) and Ohtani and Gjerloev (2020) algorithms to select against closely spaced onsets, although this would not explain the factor of ∼3 difference in yearly numbers of onsets between the two studies.

Consistent with these patterns, the multiyear statistical study by Borovsky and Yakymenko (2017) found that substorm occurrence rates were substantially higher during the declining phase of the solar cycle than they are during the other three phases of the solar cycle, and in particular that the substorm occurrence rate was greatly increased when high-speed solar wind impacted Earth (their Table 3). They also concluded that the average level of driving of the magnetosphere was highest under these conditions.

The close connection shown here between the occurrence of large GMDs and increased Vsw is also evident in Figures S3 and S4 of the supporting information for the superposed epoch study of Engebretson et al. (2021b). Figure S3 in that study showed that the medians of Vsw were relatively constant from 4 hr before to 4 hr after GMD occurrences, for both premidnight and postmidnight events and for three ranges of time delays between substorm onset and GMD occurrence, but with somewhat more variability as the number of events per station decreased from 151 down to 6. Figure S4 showed two example plots of the 8-hr Vsw traces during all the premidnight events at two representative stations, CDR and KJPK, that occurred between 0 and 30 min after the most recent substorm onset. In both plots, the number of events with Vsw values above 550 km/s exceeded those below 500 km/s. Most of the individual traces shown were rather flat over the 8-hr interval and revealed no consistent temporal pattern.

Engebretson et al. (2021b) also investigated the dependence of GMD occurrences on the solar wind dynamic pressure (Psw). The median Psw traces from 4 hr before to 4 hr after GMD occurrences were nearly flat between 2 and 3 nPa (slightly larger than the 2-year median Psw value of 1.95 nPa) for all categories except for those with 7 or fewer events (as shown in Figure 4 of that paper). Less than ∼15% of the events were associated with Psw values exceeding 5 nPa.

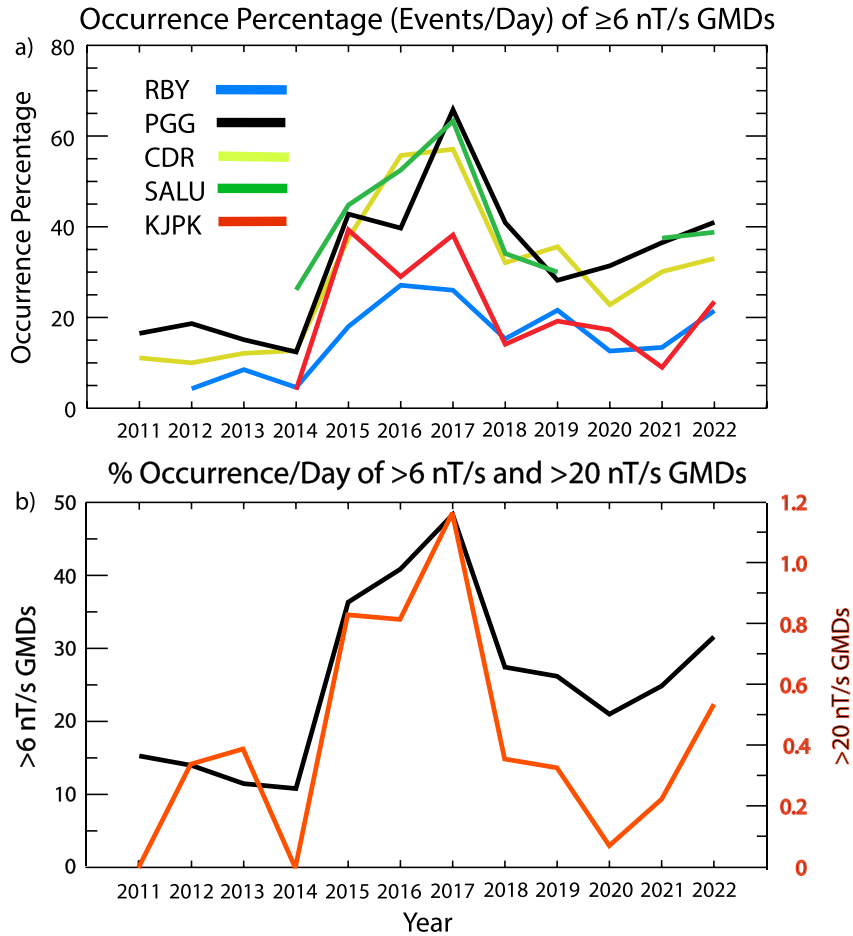

Figure 3. (a) Yearly occurrence percentages (events/station day) of ≥6 nT/s GMDs observed at each of five sites in Eastern Arctic Canada from 2011 through 2022. (b) Yearly summed occurrence percentages at all 5 sites (events/station day) of ≥6 nT/s GMDs (black trace and left vertical axis) and >20 nT/s GMDs (orange trace and right vertical axis).

4. Analysis of >20 nT/s GMDs

Figure 3 shows a comparison of the occurrence percentages of ≥6 nT/s GMDs at each of the five stations (panel a, repeated from Figure 2) to the occurrence percentage for each year of the sum of events at all five stations divided by the sum of the available station days for both ≥6 nT/s GMDs and >20 nT/s GMDs (panel b). Both traces followed roughly the Vsw and substorm trends shown in Figure 2, but the relative increase in the >20 nT/s GMD trace during 2015–2017 was much larger.

Figure 4a shows a histogram of the hourly averaged solar wind velocity (Vsw) observed during each of the >20 nT/s GMD events, and Table 3 shows the distribution of these events as a function of both year and Vsw. Figure 4b shows the distribution of all Vsw values at 1 min resolution over these same years. None of the >20 nT/s GMDs occurred when Vsw <350 km/s. Most occurred in association with the high-velocity tail of this distribution, which is well fit by a decreasing exponential. Table 3 indicates that the >20 nT/s GMDs with Vsw values above 600 km/s occurred mostly between 2015 and 2017.

Of the five >20 nT/s events with Vsw <400, two occurred during the first day of recovery after an intense CME storm, one occurred during the main phase of a modest CME storm, and one during a strong sudden impulse event before a CME storm. The fifth event, at 03:49 UT 7 December 2018, also appeared with ≥6 nT/s amplitude at three of the other four stations. It occurred during quiet conditions according to the OMNI time-shifted data base, but data from Themis D, inbound near 10 MLT from the solar wind toward the magnetopause, observed a sharp outward motion of the bow shock simultaneous with a ~20 nT negative jump in the IMF at 0358 UT (not

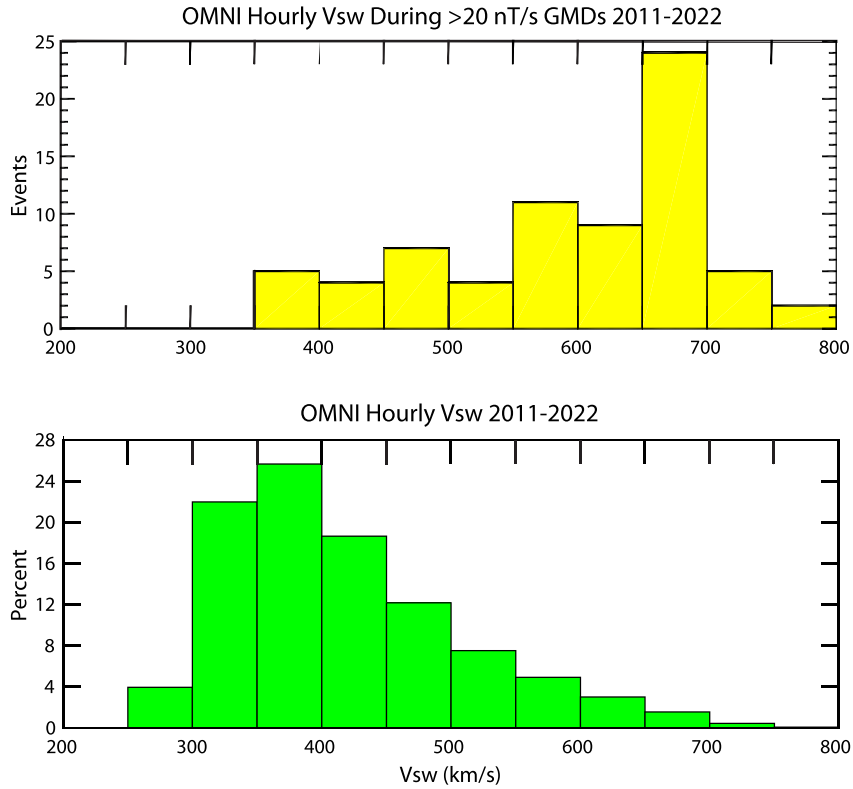

Figure 4. (a) Histogram of the distribution of hourly averaged solar wind velocities (Vsw) during >20 nT/s GMD events. (b) Histogram of the distribution of hourly averaged solar wind velocities (Vsw) from 2011 through 2022.

shown) that may have stimulated this GMD event. The Yermolaev storm list (described below) identified this event as an interplanetary shock.

Table 3
Distribution of 71 > 20 nT/s GMD Events as a Function of Year and Solar Wind Velocity (Vsw) Observed From 2011 Through 2022

Year	Vsw range 300–399	400–499	500–599	600–699	700–799	Total
2011						0
2012	1				1	2
2013			1	2		3
2014						0
2015	1		1	12		14
2016	2	2		6	1	11
2017			3	11	3	17[a]
2018	1	2	2	1		6
2019		1	3		1	5
2020			1			1
2021		1	1		1	3
2022		5	3		1	9

[a]No Vsw Data Were Available for 1 day in 2017 in the OMNI Database.

Many studies of intense or extreme dayside GMDs have noted a correlation between their occurrence and rapid increases in solar wind pressure (Psw), such as are often characteristic of sudden impulses (Sis) or sudden commencements (SCs) (e.g., Carter et al., 2015; Le et al., 1993; Oliveira et al., 2018). Table 4 shows the distribution of >20 nT/s GMDs as a function of year, Vsw below and above 500 km/s, and the presence or absence of rapid Psw increases of 1.5 nT or more from 2011 through 2022. Of these extreme GMDs, rapidly rising Psw values were associated with 6 of the 16 events (38%) that occurred when Vsw < 500 km/s, but with only 13 of the 55 events (24%) when Vsw > 500 km/s. Therefore, the majority of events for both ranges of Vsw occurred during relatively steady Psw conditions, and this pattern was even more pronounced for events when Vsw > 500 km/s.

The >20 nT/s GMD events were also sorted as functions of geomagnetic storm amplitude and phase based on the Dst index. In Table 5 GMDs are sorted into four magnetic storm categories, SI/SC events, and quiet intervals, and GMDs during storms are divided into three phases: main, recovery day 1, and recovery days 2–5. The extreme GMDs occurred most often during the main, early, and late recovery phases of moderate geomagnetic storms, weak geomagnetic storms, and quiet intervals, in that order. These patterns suggest that occurrence of these extreme GMDs was not strongly linked to either the existence, intensity, or phase of geomagnetic storms.

Table 4
Distribution of 71 > 20 nT/s GMD Events as a Function of Year, Solar Wind Velocity (Vsw) Below and Above 500 km/S, and the Presence or Absence of Rapid Solar Wind Pressure (Psw) Increases of 1.5 nT or More, From 2011 Through 2022

Year	2011	2012	2013	2014	2015	2016	2017	2018	2019	2020	2021	2022	Total
Vsw <500 km/s													
P rising	0	1	0	0	0	1	0	1	1	0	1	1	6
P steady	0	0	0	0	1	3	0	2	0	0	0	4	10
Vsw >500 km/s													
P rising	0	0	1	0	6	1	3	0	1	0	1	0	13
P steady	0	1	2	0	7	6	14	3	3	1	1	4	42
Total	0	2	3	0	14	11	17[a]	6	5	1	3	9	71

[a]No Vsw Data Were Available for 1 day in 2017 in the OMNI Database.

Table 6 shows the >20 nT/s GMD distribution based on the Yermolaev et al. (2009) list of types of solar wind as applied to the 5-min resolution OMNI data base, http://www.iki.rssi.ru/pub/omni/catalog/. All available time intervals were identified as either FAST (V > 450 km/s) or SLOW (V < 450 km/s) solar wind, and further identified, when appropriate, as forward interplanetary shocks (IS), corotating interaction regions (CIRs), and three subcategories of CMEs: ejecta, magnetic clouds, and sheath compression regions before fast ejecta or magnetic clouds. Other types listed but not represented in this data set were heliospheric current sheets, reverse interplanetary shocks, and intervals of rarefied plasma. In Table 6 we have grouped the events into seven categories: interplanetary shocks, CMEs and CIRs with slow or fast solar wind, and fast or slow solar wind not associated with either a CME or CIR. No events occurred during slow solar wind conditions not associated with either a CME or CIR. This table shows that 38 of the 72 GMDs occurred during fast solar wind conditions not during passages of CMEs or CIRs, and another 25 occurred during fast solar wind conditions during CMEs or CIRs. Only seven events occurred during intervals when Vsw < 450 km/s.

The frequent association of these GMDs with geomagnetic storms might suggest that they most often occurred during disturbed magnetospheric conditions, but analysis of their distribution as a function of SYM/H (Table 7) indicates otherwise. Only 16 of the 72 > 20 nT/s GMDs events occurred when SYM/H was ≤−51 nT. Most of these GMDs instead occurred when SYM/H was −50 nT or higher during conditions associated with weak magnetic storms or quiet conditions. The concentration of events when SYM/H was above −40 nT was strongest during 2016 and 2017, when eight out of 11 and 14 out of 18 > 20 nT/s GMDs, respectively, occurred. The patterns for 2015 and 2017 can be compared with Figure 5 of Engebretson et al. (2021a), which showed that ≥6 nT/s GMDs were also most likely to occur for SYM/H values between −40 and 0 nT. We remind readers, however, that during more intense storms the auroral oval moves much farther equatorward, out of the primary range of auroral zone magnetometers.

Table 8, presented in the same format as Table 7, shows the distribution of 1-min SME index values (the SuperMAG equivalent of AE, the auroral electrojet index) during the >20 nT/s GMDs. The yearly distributions and their sums show a peak between 800 and 1,200 nT and a broad maximum between 600 and 1,400 nT. In contrast

Table 5
Distribution of >20 nT/s GMD Events as a Function of Geomagnetic Storm Phase

Storm category	Range of Dst minimum	Main phase	Recovery day 1	Recovery days 2–5	Number of events
SI/SC					4
Major	≤−200 nT	0	0	3	3
Intense	−200 ≤ −100 nT	1	2	2	5
Moderate	−99 ≤ −50 nT	11	11	8	30
Weak	−49 ≤ −30 nT	6	11	3	20
Quiet	>−29 nT				10

Note. Definitions for the four storm categories are taken from Mursula et al. (2022).

Table 6
Distribution of GMD Events With Amplitude >20 nT/s Observed From 2011 Through 2022, Sorted Into Categories in the Yermolaev et al. (2009) List

Year	2011	2012	2013	2014	2015	2016	2017	2018	2019	2020	2021	2022	Total
IS		1						1					2
CME-S					1	3			1				5
CME-F		1	2		5		4		1		1	2	16
CIR-S						1		1					2
CIR-F			1			1	3	1				3	9
FAST					8	6	11	3	3	1	2	4	38
SLOW													0

Note. Events in the categories "Ejecta," "Magnetic Cloud," and "Sheath" are all included here under the CME heading. Both CIR and CME events are broken down further using the "Fast" and "Slow" categories (>450 or <450 km/s, respectively) into CME-F, CME-S, CIR-F and CIR-S in this table. Events are listed as "FAST" or "SLOW" only if they do not also fall into the above IS, CME, or CIR categories.

to the quiet to moderately disturbed values of the SYM/H index during these events, the SME index was never below 400 nT during these GMDs. Instead, the SME distributions indicate strong and highly variable electrojet activity and, although the small number of events in each year makes comparisons difficult, there appears to be little difference in the shape of the distributions from year to year.

Figure 5 shows the temporal relation of >20 nT/s GMD events to substorm onsets. The number of events decreased gradually with increasing time delays, but with no maximum at the time of onset or during the first 10 min. Similarly, Engebretson et al. (2021a) showed scatter plots of the amplitude of all ≥6 nT/s GMD events at five Canadian Arctic stations (the same stations except that Iqaluit was included rather than Pangnirtung) as functions of their delay after the most recent substorm onset, from 0 to 120 min and demonstrated that the number of events decreased gradually with increasing time delays at each station, with no maximum at the time of onset or during the first 10 min, consistent with the trends shown in Figure 5.

A majority of the most extreme (>20 nT/s) GMD events were also associated with higher-frequency, transient-large amplitude dB/dt intervals (TLAs) occurring prior to or within GMDs (McCuen et al., 2021). It has been recently

Table 7
Distribution of >20 nT/s GMD Events as a Function of Year and SYM/H Value Observed From 2011 Through 2022

	SYM/H range											
Year	−100–91	−90–81	−80–71	−70–61	−60–51	−50–41	−40–31	−30–21	−20–11	−10–1	0 9	Total
2011												0
2012				1							1	2
2013						1	1			1		3
2014												0
2015				2	3	3	3	3				14
2016	1	1		1			3	2	3			11
2017		1		1	1	1	4	4	6			18
2018						2	3			1		6
2019				1			3	1				5
2020									1			1
2021							1		2			3
2022				2	1		3	2	1			9
Total	1	2		8	5	7	21	12	13	2	1	72

Table 8
Distribution of >20 nT/s GMD Events as a Function of Year and SME Value Observed From 2011 Through 2022

	SME range											
Year	0	200	400	600	800	1000	1200	1400	1600	1800	2000	Total
2011												0
2012				1	1							2
2013						2			1			3
2014												0
2015				2	8	1	1	1		1		14
2016				4	2	3	2	2				11
2017			1	2	4	5	4					18
2018			2	1	1	2	1					6
2019				1	2	1						5
2020					1							1
2021			1			2						3
2022			1	1	2	2	1	1	1			9
Total	0	0	5	12	22	18	9	4	2	1		72

shown in McCuen et al. (2023) that these TLA signatures were exclusive to the auroral zone in the high magnetic latitude region. TLA events showed a very similar relation to substorm onsets as GMDs, that is, decreasing number of events with longer delay from substorm onset, but with no maximum at the time of onset.

The lack of a close temporal association between nighttime GMDs and substorm onsets has been evident in some earlier detailed studies as well. Ngwira et al. (2018) showed observations of a geomagnetic storm on 17 March 2015 during which large dB/dt events appeared from 7 to 12 min after a substorm onset, and Engebretson et al. (2019b) showed that on 11 November 2015 there was a ~10 min delay between substorm onset and the appearance of GMDs. This delay was also noted by Juusola et al. (2023) in a study of five GMD events that were responsible for the most intense derivative magnitudes in external sources (due to ionospheric and magnetospheric electric currents) observed by the IMAGE array in Scandinavia between 1994 and 2018. They found that there were no substorm onsets or sudden intensifications of the WEJ among them. They concluded that although the intensifying WEJ after substorm onset may be a typical source of moderate derivative values (as shown in Figure 3 of Viljanen et al., 2006 for ≥1 nT/s events), the rarer events with much larger derivatives tended to occur during later times.

Figure 6 shows the distribution of >20 nT/s GMD events in magnetic local time. The occurrences are dominated by a "premidnight" population from 17 MLT to near local midnight and a smaller "postmidnight" population from near local midnight to 06 MLT. The distribution is very similar to that of the much larger set of ≥6 nT/s GMD events in this region shown in Figure 4 of Engebretson et al. (2021a). It is notable that no >20 nT/s GMD events occurred between 06 and 17 MLT. These distributions are consistent with the observations of Schillings et al. (2022), who identified two "hot spots" of >±500 nT/min dB/dt spikes in the premidnight and morning magnetic local time sectors, using 1-minute cadence data from all available stations worldwide in the SuperMAG database during all magnetic storms from 1980 through 2020, independently of the geographic latitude and longitude of a given station.

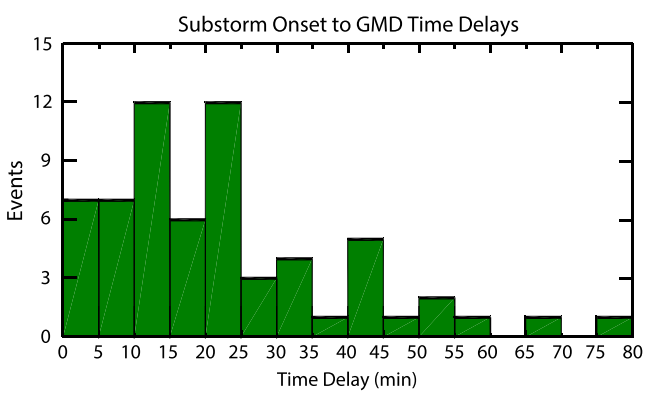

Figure 5. Histogram of the number of >20 nT/s GMD events as a function of their time delay since the most recent substorm onset listed in the SuperMAG Newell and Gjerloev (2011) catalog.

Figure 7 shows the monthly variation of large GMD occurrences. Panel a shows the average number of events per month from 2011 through 2021 (no year 2022 substorm list was available on SuperMAG as of 11 October 2023). Panel b shows the monthly average number of ≥6 nT/s GMDs after taking into account the less than complete magnetometer data coverage during several years at individual stations, and panel c shows the distribution of >20 nT/s

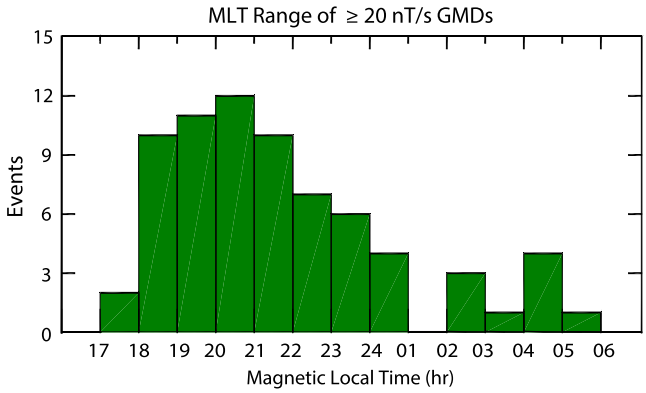

Figure 6. Histogram of the number of >20 nT/s GMD events as a function of magnetic local time (MLT).

GMDs from 2011 through 2022. The levels for SALU and KJPK are elevated compared to those at the other stations because no data were available from these two stations from 2011 through 2013, years with low numbers of GMDs at the other stations, as shown in Figure 2a. The well-known semiannual variation in substorms (Russell & McPherron, 1973) appears to hold approximately for GMDs as well (panels b and c), consistent with the frequent occurrence of GMDs after substorms.

The association between GMDs and substorm occurrences was not consistent over the solar cycle. Figure 8 shows that the annual ratio of ≥6 nT/s GMDs to substorms was smallest during the first years of sunspot Cycle 24 (between 2011 and 2014) but was larger in later years. This trend may reflect the fact that more intense substorms are associated with higher speed solar wind streams. Longer-term data from other stations or arrays may be useful for checking whether this pattern holds for previous sunspot cycles.

Table 1 shows that the separation between nearest stations in this study ranged in the north-south direction from 227 km (CDR–SALU) to 776 km

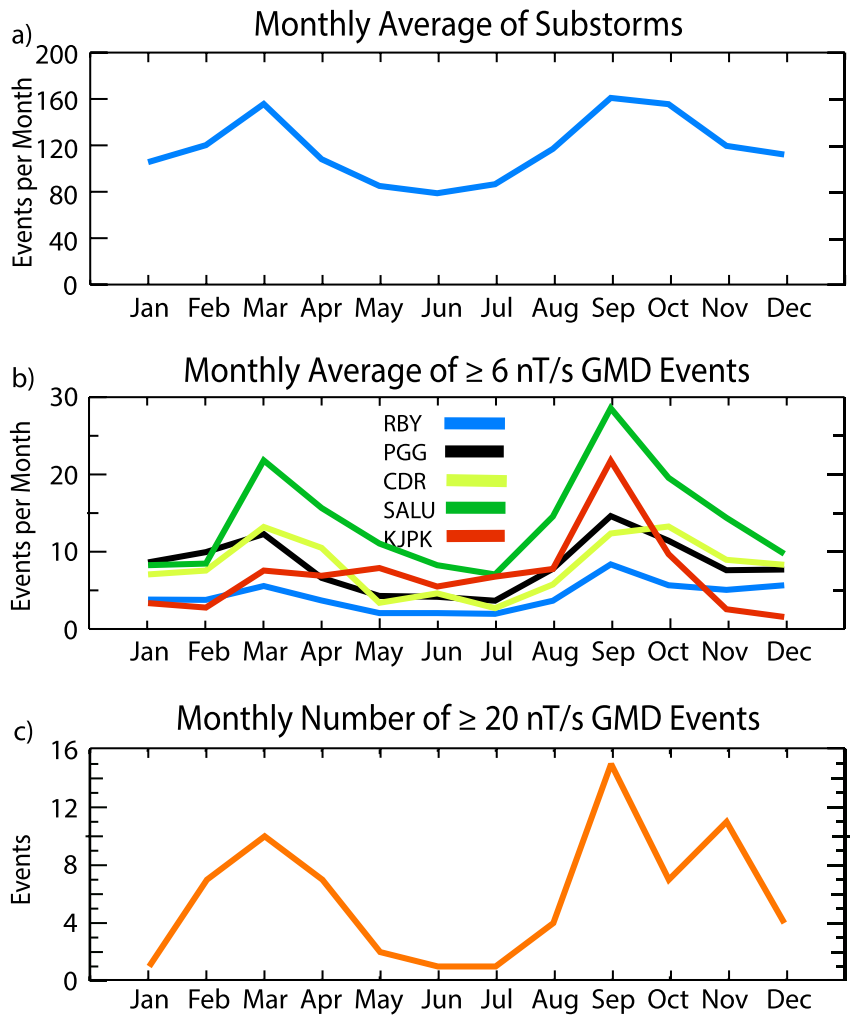

Figure 7. Monthly distributions of substorms and GMDs. Panel a shows the average number of events per month from 2011 through 2021 (no year 2022 substorm list was available on SuperMAG as of 10/11/2023). Panel b shows the weighted monthly average number of ≥6 nT/s GMDs from 2011 through 2021, and panel c shows the distribution of >20 nT/s GMDs from 2011 through 2022.

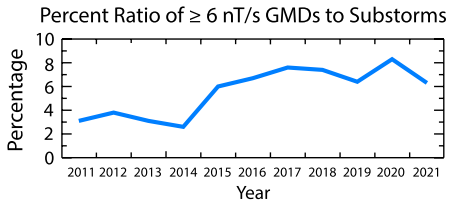

Figure 8. Plot of the percentage ratio of yearly ≥6 nT/s GMDs to the yearly number of substorms after taking into account the less than complete magnetometer coverage during several years at individual stations.

(SALU–KJPK) but were nearly equal in the east-west direction: 513 km (RBY-CDR) and 546 km (CDR-PGG). Of the 72 > 20 nT/s events, 43 (60%) were accompanied within 10 min (and often less) by events with amplitude ≥6 nT/s at one or more of the other stations in this data set. Our five-station data set includes the amplitude and time of extrema (+ and −) in all three components of the derivative at each station. We identified a probable spatial GMD progression if there was a consistent time difference in at least five of these six component extrema. Using this criterion, we identified 25 GMDs as progressing primarily northward (poleward) and one primarily westward. The remaining 17 events were stationary or unclear. In many of these latter cases large GMDs appeared only at the nearest pair of stations, CDR and SALU. The Vsw distributions of the northward, stationary, and unclear events were similar, indicating that Vsw had little or no influence regarding this spatial progression. Three similar multi-station events observed during 2015 were presented by Engebretson et al. (2019b) using stacked magnetograms, spherical elementary current systems (SECS) maps (Weygand et al., 2011) and images from a set of all-sky imagers. Two of the three showed a poleward progression. Ngwira et al. (2018) presented observations of GMDs by multiple magnetometers during two geomagnetic storms that also showed a clear poleward progression, and McCuen et al. (2023) presented a more complex event in 2016 during which separate regions of GMDs, currents, and auroras over the west and east coasts of Hudson Bay both showed a poleward progression. We discuss possible mechanisms causing these poleward progressions below.

5. Comparison to Three Other Studies of Multiyear GMD Data Sets

We are aware of three other studies of GMDs that span one or more recent solar cycles. Milan et al. (2023) presented a comprehensive survey of >300 nT perturbations in any component of the magnetic fields in 1 min cadence data from all available magnetometer stations above 50° magnetic latitude in the SuperMAG data base from 1995 to 2020. Kellinsalmi et al. (2022) compiled the distribution of >1 nT/s GMDs observed at Sodankylä, Finland from 1996 through 2018, and Marshall et al. (2011) presented GMD activity index data from 1985 through 2009 from several sites across Australia. The solar cycle occurrence patterns observed by these studies, with maxima during the declining phase, were all similar to those presented here.

Milan et al. (2023) cataloged all instances of minute-to-minute changes in magnetic field components ("spikes") that exceeded 300 nT, which corresponds to a derivative threshold of 5 nT/s. Although several earlier studies (e.g., Engebretson et al., 2019a, 2021b; Viljanen, 1997; Viljanen et al., 2006) reported a lack of good correlation between ΔB and dB/dt amplitudes during large MPEs, these perturbations remain a useful proxy for GMDs, especially when higher time resolution data are not available. Milan et al. (2023) identified two local time regions of greatest activity: premidnight (17–02 MLT) and postmidnight (02–09 MLT), consistent with the observations of Engebretson et al. (2021a) and Schillings et al. (2022). They noted maximum occurrence rates during the declining phases of both Solar Cycles 23 and 24, and their Figure 3 showed similar occurrence trends in spikes and high-speed streams. Based on a comparison of yearly spike occurrences in Figure 3a that showed similar patterns using thresholds of 100, 200, 300, and 400 nT/min, Milan et al. (2023) suggested that their shapes did not depend on the magnitude of the spikes. However, although the timing of these patterns did not change, the ratio of maxima to minima using these different thresholds increased from the >100 nT/min trace to the >400 nT/min trace. We observed a similar trend in data presented in Table 2 and Figure 3b above for ≥6 and >20 nT/s events; the temporal patterns were again similar, but the amplitude of their variations increased with increasing thresholds, even for extreme GMDs.

Kellinsalmi et al. (2022) included the annual totals of >1 nT/s GMDs recorded at Sodankylä, Finland (63.9° MLAT) in their Figure 7. A comparison of panels a and b of Figure 9 here shows that the trend in the annual total of these >1 nT/s GMDs was similar to that in sunspots between 1996 and 2001 (the rising part of sunspot Cycle 23), and during the sunspot minimum years and early part of Cycle 24, between 2006 and 2012. However, the sharp peak in GMDs during 2003 matched well with sharp peaks in Vsw (panel c) and substorms (panel d), while there was no corresponding peak in sunspots (panel b). Subsidiary peaks in GMDs in 2005 and 2017 also matched those in Vsw and substorms but not sunspots, and the relative minima in GMDs during 2001 and 2002 matched similar minima in Vsw and substorms rather than the simultaneous rise in sunspots. We note that the

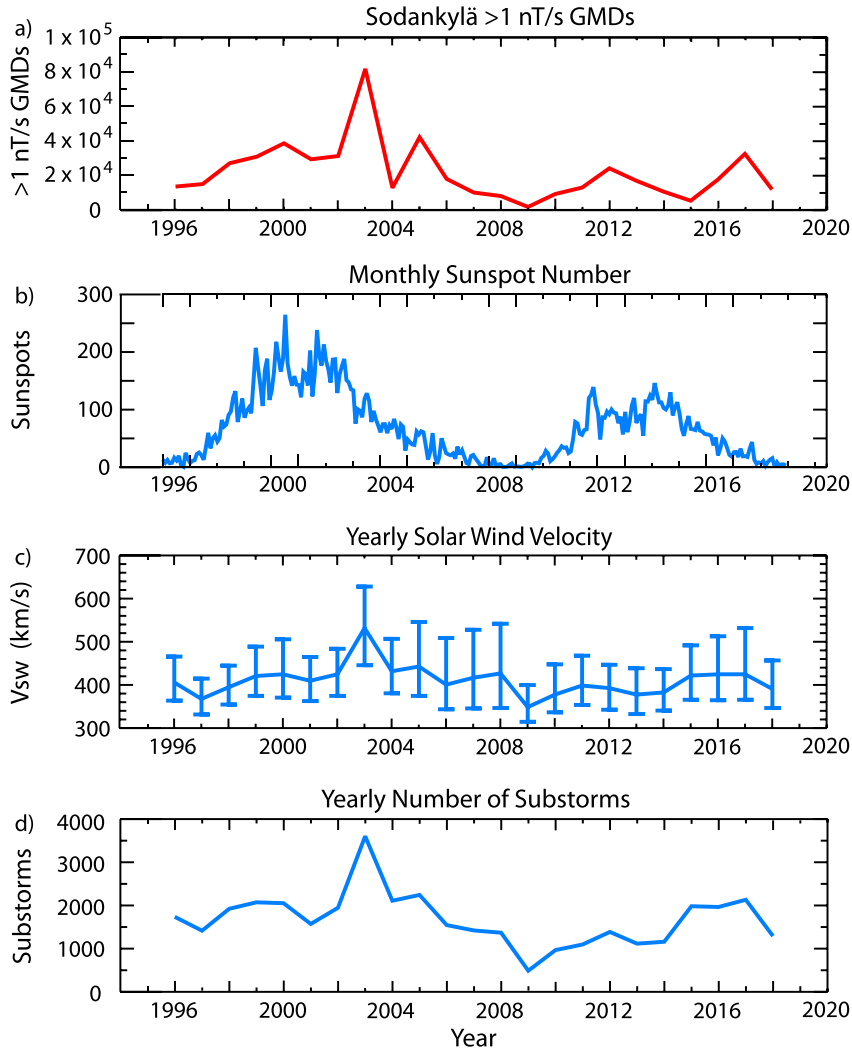

Figure 9. (a) Yearly numbers of ≥1 nT/s GMDs observed at Sodankylä, Finland from 1996 through 2018. (b) Monthly sunspot numbers from January 1996 through December 2018. (c) Yearly medians and 25th and 75th percentile values (lower and upper bars) of the solar wind velocity and (d) Yearly averages of the number of substorm onsets, respectively, from 1996 through 2018, again taken from the Newell and Gjerloev (2011) SuperMAG substorm list.

75th percentile values were further from the median than the 25th percentile values during 2003 and 2005–2008, again indicating a more extended high-velocity tail of the Vsw distributions during those years, but that there were fewer substorms and also fewer GMDs during 2006–2008. As noted above, the smaller GMD threshold of >1 nT/s allows the inclusion of many substorm onsets in the GMD count, so the decrease in GMD activity during these three years may primarily reflect the decrease in the number of substorms.

An earlier study by Marshall et al. (2011) also showed similarities to the patterns presented above at lower latitudes, ranging from −22.7° to −50.7° magnetic latitude, from 1985 through 2009. Figure 10a, adapted from Figure 7 of Marshall et al. (2011), shows the values of their GICy index, a frequency domain filter applied to geomagnetic field data recorded at seven stations across Australia to determine GIC risk level thresholds. The horizontal yellow and orange lines are the lower limit thresholds for the "low" and "moderate" threat levels defined in that study. The colored symbols in Figure 10a show GICy index values for every event exceeding the threshold for "low" risk, and the pink trace shows the sunspot number during these same years. The highest latitude station, Hobart, Tasmania (symbols in dark blue), only had data available for the second solar cycle. Figure 10b shows the annual Vsw averages and percentiles, and Figure 10c shows the annual number of substorms, again from the Newell and Gjerloev (2011)-based SuperMAG list.

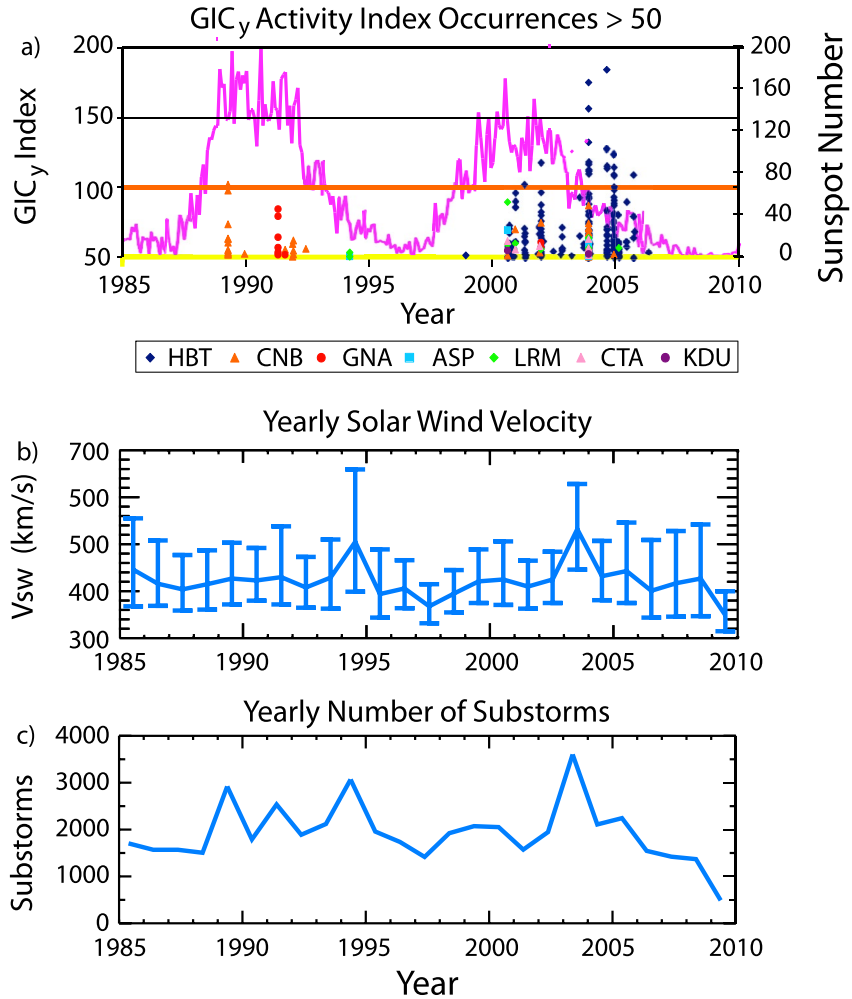

Figure 10. (a) Adapted version of Figure 7 of Marshall et al. (2011), showing GICy indices >50 from magnetometer locations across Australia (colored dots, corresponding to the vertical scale on the left side) and the solar sunspot number (pink trace, corresponding to the vertical scale on the right), from 1985 through 2009. The horizontal yellow and orange lines are the lower limit thresholds for the "low" and "moderate" threat levels defined in that study. (b) Yearly medians and 25th and 75th percentile values (lower and upper bars) of the solar wind velocity and (c) Yearly numbers of substorm onsets from the Newell and Gjerloev (2011) list on SuperMAG, respectively, from 1985 through 2009.

During 1989 (the end of the rising phase of the solar cycle) and 1991 (the beginning of the declining phase) GMDs with GICy values >50 occurred when all three of sunspot numbers, annual Vsw averages, and annual substorm averages had relative maxima. The two index values near 100 in 1989 reached the moderate risk level and occurred during the 13 March 1989 superstorm. We note that the 75th percentile value of Vsw during 1991 was comparable to those during the declining phase of Cycle 23, again indicating a longer high velocity tail.

Only one GICy ~50 event (just above the low-risk threshold) occurred during the rising phase of the next sunspot cycle (from 1997 through 2000), but a large number of events occurred during the declining phase (from late 2000 through 2006). Most of these events were observed at Hobart, including 21 events over nine different days in the moderate risk range.

We also note that although the peaks of Vsw and substorms were both largest in 1994 and 2003, no GMDs were observed at Australian stations during 1994, and the number of GMD events between late 2000 and the end of 2006 was high, their annual variations did not follow closely the variations in Vsw or substorms. The lack of correlation with substorm onsets may be due to the location of these stations far from the auroral zone, but the lack of correlation with increased levels of Vsw does not necessarily follow from this observation. This data set thus shows both the strong dependence of GMDs on the phase of the sunspot cycle (most clearly seen at the

mid-latitude Hobart station) and the probable multiplicity of driving factors that may govern their occurrence in regions equatorward of the auroral zone.

6. Discussion

We have noted above not only the strong connection between intense GMDs and high-speed solar wind streams, as has been found in several other studies, but the frequent poleward progression of these GMDs. We here review recent studies that may indicate the physical connection between these two phenomena.

Tsurutani and Gonzalez (1987) and Tsurutani et al. (2011) concluded that the major cause of geomagnetic activity during extended HILDCAA intervals, associated with high-speed solar wind streams, is large amplitude Alfvén waves. Dai et al. (2023) confirmed these findings in multiple events in corotating interaction region-driven geomagnetic storms. They noted that Alfvénic fluctuations in the solar wind associated with repetitive substorms contributed to the extended recovery phases of geomagnetic storms, and that such intervals were promptly followed by hundreds of nT increases in the AE and AU auroral electrojet indices within 10–20 min. Dai et al. (2023) also presented a phenomenological model of strongly driven substorms, in which the increase of the AE index is linked to dayside reconnection mainly through the ionosphere (through enhanced two-cell convection) instead of the magnetotail, and suggested that this pattern is expected to be particularly viable and even dominant in the descending phase of the solar cycle.

Earlier studies by Kim et al. (2009) and Lyons et al. (2009) also found evidence for links between dayside reconnection and nightside disturbances via increased ionospheric convection. Kim et al. (2009) noted that north-south solar wind fluctuations enhanced ionospheric convection flows in the dayside polar cap and that ULF power in the solar wind enhanced the convection strength, independent of an observed direct effect from the solar wind speed. They also noted that these large oscillations of convection flow speeds occurred independent of the direction of the IMF, found correlations with Vsw and Psw, and presented evidence that the power in the IMF fluctuations affects the convection independently of effects of Psw fluctuations. Lyons et al. (2009) found that there were also close relationships between solar wind fluctuations and convection flows in the nightside ionosphere and within the plasma sheet, indicating that the effect of the solar wind fluctuations was global.

Lyons et al. (2011, 2013) extended this connection to auroral poleward expansions, post-onset auroral streamers, and the duration of post-onset auroral activity. Lyons et al. (2013) noted that the more abrupt and larger magnetic field responses came not from auroral onsets but in association with post-onset streamers at times varying from just a few minutes to well over 30 min after substorm auroral onset if there was a prolonged period of streamers. Similarly, Nishimura et al. (2013) presented evidence indicating that plasma transport (observed as airglow patches) originating from the dayside and reaching the nightside open-closed boundary may trigger plasma sheet flow bursts and play a crucial role in both pre- and post-onset auroral activity.

The poleward progression of these GMDs and associated increases in ionospheric and field-aligned currents are related to the tailward retreat of the magnetotail reconnection region, as suggested in observational studies by Nakamura et al. (2011) and Ieda et al. (2016). The reconnection region associated with a substorm onset may initially be close to Earth, but as the magnetic field dipolarizes, subsequent auroral breakups correspond to reconnection regions farther downtail. This tailward retreat corresponds to the poleward shift of the magnetic footprint.

A recent study by Zou et al. (2022) used coordinated observations from THEMIS and Geophysical Institute Magnetometer Array magnetometers and THEMIS all-sky imagers to statistically examine large dB/dt intervals during geomagnetic storms from 2015 to 2016. They identified a variety of auroral drivers, including poleward expanding auroral bulges, auroral streamers, poleward boundary intensifications, omega bands, and pulsating auroras. In particular, they noted that poleward expanding auroral bulges drive large dB/dt events that spread progressively poleward, and periodic injections of streamers drive large dB/dt events that occurred in periodic bursts.

Although the importance of the auroral drivers for GMDs suggested by Zou et al. (2022) is consistent with this study and our previous studies, we have found that these auroral drivers are not limited to the occurrences of geomagnetic storms. Instead, the most intense nighttime GMDs at high latitudes and extending toward midlatitudes are related statistically to substorms and especially extended periods of magnetotail activity related to

high-speed streams. Two of the three events presented by Engebretson et al. (2019b) noted the association between intense GMDs and auroral streamers, as did one event shown in Figure 11 of Weygand et al. (2021).

7. Summary and Conclusions

This study has presented observations of ≥6 and >20 nT/s GMD occurrences at high latitudes (nearly all of them during local nighttime) during the most recent sunspot cycle and compared them to several parameters that are expected to be associated with them: a measure of solar activity (monthly sunspot numbers), measures of the interaction between the solar wind and the magnetosphere (the solar wind velocity Vsw and dynamic pressure Psw), a measure of activity in the magnetotail (the number of substorm onsets), and a measure of magnetic storm intensity (the SYM/H index). Our previous studies have shown a strong short-term relation between the occurrence of ≥6 nT/s GMDs and prior ∼30 min intervals of southward IMF Bz, which is also related to magnetotail activity and the occurrence of substorm onsets.

1. In the data sets presented here, GMDs ≥6 nT/s occurred more often during the declining phase of sunspot cycles, rather than during their first half or during years of sunspot maxima or minima. This was evident for GMDs observed in Arctic Canada between 2011 and 2022 (this study) and was consistent in large part with three published studies using data covering multiple years. It is notable that even at mid- and low latitudes, many more GMDs occurred during the declining phase of the sunspot cycle, but we noted that very few events were observed in Australia during any part of the 1988–1997 solar cycle.
2. The annual GMD occurrence percentages in this study agreed better with annual values of the solar wind velocity, and only slightly less well with annual average values of substorm occurrences. Many or most of these GMDs were associated with high-speed solar wind streams that can occur either in association with geomagnetic storms stimulated by high-speed CMEs or CIRs or during their extended aftermath, during HILDCAA intervals.
3. Occurrences of >20 nT/s GMDs in this study were more strongly associated with the declining phase of the sunspot cycle and with high Vsw values than ≥6 nT/s GMDs. Occurrences of >20 nT/s GMDs were most common within 25 min after a substorm onset (but few occurred within 5 min), and all occurred within 80 min after an onset. These timing patterns appeared also in our earlier studies of ≥6 nT/s GMDs. Occurrences of these GMDs showed a peak in the SYM/H range from −40 to −11, that is, mostly during modestly or weakly disturbed geomagnetic conditions, but as noted above, during more intense magnetic storms the auroral oval moves much farther equatorward, so large GMDs would tend to be observed less often at high latitudes.
4. Of the 43 of 72 >20 nT/s GMD events that were also observed with large amplitude at neighboring stations, 25 showed a poleward progression, one a westward progression, 17 were stationary or unclear, and none were equatorward. The mechanisms governing this poleward progression may be related to auroral poleward expansion, which may be attributed to the tailward retreat of the magnetotail reconnection region, which is now known to occur during times of roughly continuous disturbed conditions stimulated by high-speed solar wind streams and their associated Alfvén waves.

The combination of the strong connection between intense and extreme GMD events at high latitudes and both high-speed solar wind streams and intervals following substorm onsets, rather than with intense magnetic storms and large negative SYM/H values, as well as the relative absence of such events during the rising phase of the last three solar cycles, suggests that warnings of intense GMDs should not be restricted to the rising phase of the sunspot cycle or times when CMEs are approaching Earth. Rather, the relatively less studied occurrence of high-speed solar wind streams and HILDCAA activity that are associated with geomagnetically disturbed conditions during the declining phase of the sunspot cycle may provide additional clues as to the proximate causes of these often impulsive nighttime disturbances.

Data Availability Statement

Ground-based magnetometer data used in this multi-year study were recorded at five stations in the MACCS (Engebretson et al., 2011) and AUTUMNX (Connors, 2023) arrays in Eastern Arctic Canada. The database of GMD events created in this study is available in the University of Michigan Deep Blue Data Repository (Engebretson, 2023). The three substorm lists accessed in this study are available from the SuperMAG web site (Gjerloev, 2023). OMNI data are available from the Coordinated Data Analysis Web (CDAWeb) part of the Space

Physics Data Facility at the NASA Goddard Space Flight Center (Papitashvili & King, 2020). The Yermolaev list of solar wind phenomena and related documentation is available from a web site provided by the Space Research Institute (IKI), Moscow (Yermolaev, 2023).

Acknowledgments
We thank David Boteler, Shin Ohtani, and Jesper Glerloev for helpful discussions. This research was supported by National Science Foundation Grants AGS-2013648 to Augsburg University and AGS-2013433 to the University of Michigan. Martin G. Connors thanks NSERC for research support and the Canadian Space Agency for support of AUTUMNX. Work by James M. Weygand was supported by NASA Grants HSR-80NSSC18K1227 and SWO2R 80NSSC20K1364, NASA contract HPDE-80GSFC17C0018, NSF Grant GEO-NERC 2027190, and NSF Grant AGS-2013648 via subcontract from Augsburg University. Work by Larry R. Lyons was supported by NSF Grants AGS-20191955 and AGS-2055192 and NASA Grants 80NSSC20K1314 and 80NSSC22K0749. Work by Yukitoshi Nishimura was supported by NASA Grants 80NSSC18K0657, 80NSSC20K0604, 80NSSC20K0725, 80NSSC21K1321, 80NSSC22K0323, and 80NSSC22M0104, NSF Grants AGS-1907698 and AGS-2100975, and AFOSR Grant FA9559-16-1-0364. THEMIS is supported by NASA NAS5-02099 and the Canadian Space Agency.

References

Al Shidi, Q., Pulkkinen, T., Toth, G., Brenner, A., Zou, S., & Gjerloev, J. (2022). A large simulation set of geomagnetic storms—Can simulations predict ground magnetometer station observations of magnetic field perturbations? *Space Weather*, *20*(11), e2022SW003049. https://doi.org/10.1029/2022SW003049

Arajärvi, E., Pirjola, R. J., & Viljanen, A. (2011). Effects of neutral point reactors and series capacitors on geomagnetically induced currents in a high-voltage electric power transmission system. *Space Weather*, *9*(11), S11005. https://doi.org/10.1029/2011SW000715

Borovsky, J. E., & Denton, M. H. (2006). Differences between CME-driven storms and CIR-driven storms. *Journal of Geophysical Research*, *111*(A7), A07S08. https://doi.org/10.1029/2005JA011447

Borovsky, J. E., & Yakymenko, K. (2017). Substorm occurrence rates, substorm recurrence times, and solar wind structure. *Journal of Geophysical Research: Space Physics*, *122*(3), 2973–2998. https://doi.org/10.1002/2016JA023625

Boteler, D. H. (2001). Assessment of geomagnetic hazard to power systems in Canada. *Natural Hazards*, *23*(2/3), 101–120. https://doi.org/10.1023/A:1011194414259

Boteler, D. H. (2019). A 21st century view of the March 1989 magnetic storm. *Space Weather*, *17*(10), 1427–1441. https://doi.org/10.1029/2019SW002278

Boteler, D. H., & Pirjola, R. J. (2017). Modeling geomagnetically induced currents. *Space Weather*, *15*(1), 258–276. https://doi.org/10.1002/2016SW001499

Boteler, D. H., Pirjola, R. J., & Nevanlinna, H. (1998). The effects of geomagnetic disturbances on electrical systems at the Earth's surface. *Advances in Space Research*, *22*(1), 17–27. https://doi.org/10.1016/S0273-1177(97)01096-X

Carrington, R. C. (1859). Description of a singular appearance seen in the Sun on September 1, 1859. *Monthly Notices of the Royal Astronomical Society*, *20*, 13–15. https://doi.org/10.1093/mnras/20.1.13

Carter, B. A., Yizengaw, E., Pradipta, R., Halford, A. J., Norman, R., & Zhang, K. (2015). Interplanetary shocks and the resulting geomagnetically induced currents at the equator. *Geophysical Research Letters*, *42*(16), 6554–6559. https://doi.org/10.1002/2015GL65060

Cliver, E. W., & Dietrich, W. F. (2013). The 1859 space weather event revisited: Limits of extreme activity. *Journal of Space Weather and Space Climate*, *3*, 31. https://doi.org/10.1051/swsc/2013053

Connors, M., Schofield, I., Reiter, K., Chi, P. J., Rowe, K. M., & Russell, C. T. (2016). The AUTUMNX magnetometer meridian chain in Québec, Canada. *Earth Planets and Space*, *68*(1), 2. https://doi.org/10.1186/s40623-015-0354-4

Connors, M. G. (2023). AUTUMNX Athabasca university THEMIS UCLA magnetometer network [Dataset]. Athabasca University, Canada. https://autumn.athabascau.ca

Dai, L., Han, Y., Wang, C., Yao, S., Gonzalez, W. D., Duan, S., et al. (2023). Geoeffectiveness of interplanetary Alfvén Waves, I, Magnetopause magnetic reconnection and directly driven substorms. *The Astrophysical Journal*, *945*(1), 47. https://doi.org/10.3847/1538-4357/acb267

Dimmock, A. P., Rosenqvist, L., Hall, J.-O., Viljanen, A., Yordanova, E., Honkonen, I., et al. (2019). The GIC and geomagnetic response over Fennoscandia to the 7–8 September 2017 geomagnetic storm. *Space Weather*, *17*(7), 989–1010. https://doi.org/10.1029/2018SW002132

Dimmock, A. P., Rosenqvist, L., Welling, D. T., Viljanen, A., Honkonen, I., Boynton, R. J., & Yordanova, E. (2020). On the regional variability of dB/dt and its significance to GIC. *Space Weather*, *18*(8), e2020SW002497. https://doi.org/10.1029/2020SW002497

Engebretson, M., Steinmetz, E., & Moldwin, M. (2011). MACCS 0.5 s ground magnetometer data [Dataset]. Augsburg University. https://doi.org/10.48322/sydj-ab90

Engebretson, M. J. (2023). Solar cycle dependence of very large nighttime geomagnetic disturbances (GMDs) observed in eastern Arctic Canada: Data [Dataset]. University of Michigan - Deep Blue Data. https://doi.org/10.7302/275e-da06

Engebretson, M. J., Ahmed, L. Y., Pilipenko, V. A., Steinmetz, E. S., Moldwin, M. B., Connors, M. G., et al. (2021b). Superposed epoch analysis of nighttime magnetic perturbation events observed in Arctic Canada (2021). *Journal of Geophysical Research: Space Physics*, *126*(9), e2021JA029465. https://doi.org/10.1029/2021JA029465

Engebretson, M. J., Hughes, W. J., Alford, J. L., Zesta, E., Cahill, L. J., Jr., Arnoldy, R. L., & Reeves, G. D. (1995). Magnetometer array for cusp and cleft studies observations of the spatial extent of broadband ULF magnetic pulsations at cusp/cleft latitudes. *Journal of Geophysical Research*, *100*(A10), 19371–19386. https://doi.org/10.1029/95JA00768

Engebretson, M. J., Pilipenko, V. A., Ahmed, L. Y., Posch, J. L., Steinmetz, E. S., Moldwin, M. B., et al. (2019a). Nighttime magnetic perturbation events observed in Arctic Canada: 1. Survey and statistical analysis. *Journal of Geophysical Research: Space Physics*, *124*(9), 7442–7458. https://doi.org/10.1029/2019JA026794

Engebretson, M. J., Pilipenko, V. A., Steinmetz, E. S., Moldwin, M. B., Connors, M. G., Boteler, D. H., et al. (2021a). Nighttime magnetic perturbation events observed in Arctic Canada: 3. Occurrence and amplitude as functions of magnetic latitude, local time, and magnetic disturbances. *Space Weather*, *19*, e2020SW002526. https://doi.org/10.1029/2020SW002526

Engebretson, M. J., Steinmetz, E. S., Posch, J. L., Pilipenko, V. A., Moldwin, M. B., Connors, M. G., et al. (2019b). Nighttime magnetic perturbation events observed in Arctic Canada: 2. Multiple-instrument observations. *Journal of Geophysical Research: Space Physics*, *124*(9), 7459–7476. https://doi.org/10.1029/2019JA026797

Forsyth, C., Rae, I. J., Coxon, J. C., Freeman, M. P., Jackman, C. M., Gjerloev, J., & Fazakerley, A. N. (2015). A new technique for determining substorm onsets and phases from indices of the electrojet (SOPHIE). *Journal of Geophysical Research: Space Physics*, *120*(12), 10592–10606. https://doi.org/10.1002/2015JA021343

Gannon, J. L., Swidinsky, A., & Xu, Z. (Eds.), (2019). Geomagnetically induced currents from the Sun to the power grid. *Geophysical Monograph Series*, (Vol. 244). https://doi.org/10.1002/9781119434412

Gjerloev, J. W. (2023). SuperMAG, Global magnetic field observations and products made possible by the contributors [Dataset]. SuperMAG. https://supermag.jhuapl.edu/

Haiducek, J. D., Welling, D. T., Ganushkina, N. Y., Morley, S. K., & Ozturk, D. S. (2017). SWMF global magnetosphere simulations of January 2005: Geomagnetic indices and cross-polar cap potential. *Space Weather*, *15*(12), 1567–1587. https://doi.org/10.1002/2017SW001695

Hapgood, M. (2019). The Great storm of May 1921: An exemplar of a dangerous space weather event. *Space Weather*, *17*(7), 950–975. https://doi.org/10.1029/2019SW002195

Ieda, A., Nishimura, Y., Miyashita, Y., Angelopoulos, V., Runov, A., Nagai, T., et al. (2016). Stepwise tailward retreat of magnetic reconnection: THEMIS observations of an auroral substorm. *Journal of Geophyical Research: Space Physics*, *121*(5), 4548–4568. https://doi.org/10.1002/2015JA022244

Iijima, T., & Potemra, T. A. (1978). Large-scale characteristics of field-aligned currents associated with substorms. *Journal of Geophysical Research*, *83*(A2), 599–615. https://doi.org/10.1029/JA083iA02p00599

Juusola, L., Viljanen, A., Dimmock, A. P., Kellinsalmi, M., Schillings, A., & Weygand, J. M. (2023). Drivers of rapid geomagnetic variations at high latitudes. *Annales Geophysicae*, *41*(1), 13–37. https://doi.org/10.5194/angeo-41-13-2023

Kappenman, J. G. (2005). An overview of the impulsive geomagnetic field disturbances and power grid impacts associated with the violent Sun-Earth connection events of 29--31 October 2003 and a comparative evaluation with other contemporary storms. *Space Weather*, *3*(8), S08C01. https://doi.org/10.1029/2004SW000128

Kappenman, J. G. (2006). Great geomagnetic storms and extreme impulsive geomagnetic field disturbance events—An analysis of observational evidence including the great storm of May 1921. *Advances in Space Research*, *38*(2), 188–199. https://doi.org/10.1016/j.asr.2005.08.055

Kellinsalmi, M., Viljanen, A., Juusola, L., & Käki, S. (2022). The time derivative of the geomagnetic field has a short memory. *Annals of Geophysics*, *40*(4), 545–562. https://doi.org/10.5194/angeo-40-545-2022

Kim, H.-J., Lyons, L. R., Zou, S., Boudouridis, A., Lee, D.-Y., Heinselman, C., & McCready, M. (2009). Evidence that solar wind fluctuations substantially affect the strength of dayside ionospheric convection. *Journal of Geophysical Research*, *114*(A11), A11305. https://doi.org/10.1029/2009JA014280

Kwagala, N., Hesse, M., Moretto, T., Tenfjord, P., Norgren, C., Toth, G., et al. (2020). Validating the space weather modeling framework (SWMF) for applications in northern Europe: Ground magnetic perturbation validation. *Journal of Space Weather and Space Climate*, *10*, 1–13. https://doi.org/10.1051/swsc/2020034

Le, G., Russell, C. T., Petrinec, S. M., & Ginskey, M. (1993). Effect of sudden solar wind dynamic pressure changes at subauroral latitudes: Change in magnetic field. *Journal of Geophysical Research*, *98*(A3), 3983–3990. https://doi.org/10.1029/92ja02397

Liemohn, M., Ganushkina, N. Y., De Zeeuw, D. L., Rastaetter, L., Kuznetsova, M., Welling, D. T., et al. (2018). Real-time SWMF at CCMC: Assessing the Dst output from continuous operational simulations. *Space Weather*, *16*(10), 1583–1603. https://doi.org/10.1029/2018SW001953

Love, J. J., Hayakawa, H., & Cliver, E. W. (2019). Intensity and impact of the New York railroad superstorm of May 1921. *Space Weather*, *17*(8), 1281–1292. https://doi.org/10.1029/2019SW002250

Lyons, L. R., Kim, H.-J., Xing, X., Zou, S., Lee, D. Y., Heinselman, C., et al. (2009). Evidence that solar wind fluctuations substantially affect global convection and substorm occurrence. *Journal of Geophysical Research*, *114*(A11), A11306. https://doi.org/10.1029/2009JA014281

Lyons, L. R., Nishimura, Y., Donovan, E., & Angelopoulos, V. (2013). Distinction between auroral substorm onset and traditional ground magnetic onset signatures. *Journal of Geophysical Research: Space Physics*, *118*(7), 4080–4092. https://doi.org/10.1002/jgra.50384

Lyons, L. R., Nishimura, Y., Kim, H.-J., Donovan, E., Angelopoulos, V., Sofko, G., et al. (2011). Possible connection of polar cap flows to pre- and post-substorm onset PBIs and streamers. *Journal of Geophysical Research*, *116*(A12), A12225. https://doi.org/10.1029/2011JA016850

Mac Manus, D. H., Rodger, C. J., Dalzell, M., Renton, A., Richardson, G. S., Petersen, T., & Clilverd, M. A. (2022). Geomagnetically induced current modeling in New Zealand: Extreme storm analysis using multiple disturbance scenarios and industry provided hazard magnitudes. *Space Weather*, *20*(12), e2022SW003320. https://doi.org/10.1029/2022SW003320

Marshall, R. A., Smith, E. A., Francis, M. J., Waters, C. L., & Sciffer, M. D. (2011). A preliminary risk assessment of the Australian region power network to space weather. *Space Weather*, *9*(10), S10004. https://doi.org/10.1029/2011SW000685

McCuen, B. A., Moldwin, M. B., & Engebretson, M. J. (2021). Characterization of transient-large-amplitude geomagnetic perturbation events. *Geophysical Research Letters*, *48*(15), e2021GL094076. https://doi.org/10.1029/2021GL094076

McCuen, B. A., Moldwin, M. B., Engebretson, M. J., Weygand, J. M., & Nishimura, Y. (2023). Magnetosphere–ionosphere drivers of transient-large amplitude geomagnetic disturbances: Statistical analysis and event study. *Journal of Geophysical Research: Space Physics*, *128*(11), e2023JA031587. https://doi.org/10.1029/2023JA031587

Milan, S. E., Imber, S. M., Fleetham, A. L., & Gjerloev, J. (2023). Solar cycle and solar wind dependence of the occurrence of large *dB/dt* events at high latitudes. *Journal of Geophysical Research: Space Physics*, *128*(4), e2022JA030953. https://doi.org/10.1029/2022JA030953

Molinski, T. S., Feero, W. E., & Damsky, B. L. (2000). Shielding grids from solar storms. *IEEE Spectrum*, *37*(11), 55–60. https://doi.org/10.1109/6.880955

Morley, S. K. (2020). Challenges and opportunities in magnetospheric space weather prediction. *Space Weather*, *18*(3), e2018SW002108. https://doi.org/10.1029/2018SW002108

Mursula, K., Qvick, T., Holappa, L., & Asikainen, T. (2022). Magnetic storms during the space age: Occurrence and relation to varying solar activity. *Journal of Geophysical Research: Space Physics*, *127*(12), e2022JA030830. https://doi.org/10.1029/2022JA030830

Nakamura, R., Baumjohann, W., Panov, E., Petrukovich, A. A., Angelopoulos, V., Volwerk, M., et al. (2011). Flux transport, dipolarization, and current sheet evolution during a double-onset substorm. *Journal of Geophysical Research*, *116*(A5), A00I36. https://doi.org/10.1029/2010JA015865

Newell, P. T., & Gjerloev, J. W. (2011). Evaluation of SuperMAG auroral electrojet indices as indicators of substorms and auroral power. *Journal of Geophysical Research*, *116*(A12), A12211. https://doi.org/10.1029/2011JA016779

Ngwira, C. M., & Pulkkinen, A. A. (2019). An introduction to geomagnetically induced currents. In J. L. Gannon, A. Swidinsky, & Z. Xu (Eds.), *Geomagnetically induced currents from the Sun to the power grid*, *Geophysical Monograph Series* (Vol. 244, pp. 3–13). American Geophysical Union. https://doi.org/10.1002/9781119434412.ch1

Ngwira, C. M., Sibeck, D., Silveira, M. D. V., Georgiou, M., Weygand, J. M., Nishimura, Y., & Hampton, D. (2018). A study of intense local dB/dt variations during two geomagnetic storms. *Space Weather*, *16*(6), 676–693. https://doi.org/10.1029/2018SW001911

Nishimura, Y., Lyons, L. R., Shiokawa, K., Angelopoulos, V., Donovan, E. F., & Mende, S. B. (2013). Substorm onset and expansion phase intensification precursors seen in polar cap patches and arcs. *Journal of Geophysical Research: Space Physics*, *118*(5), 2034–2042. https://doi.org/10.1002/jgra.50279

Ohtani, S., & Gjerloev, J. W. (2020). Is the substorm current wedge an ensemble of wedgelets? Revisit to midlatitude positive bays. *Journal of Geophysical Research: Space Physics*, *125*(9), e2020JA027902. https://doi.org/10.1029/2020JA027902

Oliveira, D. M., Arel, D., Raeder, J., Zesta, E., Ngwira, C. M., Carter, B. A., et al. (2018). Geomagnetically induced currents caused by interplanetary shocks with different impact angles and speeds. *Space Weather*, *16*(6), 636–647. https://doi.org/10.1029/2018SW001880

Papitashvili, N. E., & King, J. H. (2020). OMNI 1-min data" [Dataset]. NASA Space Physics Data Facility. https://doi.org/10.48322/45bb-8792

Pilipenko, V., Kozyreva, O., Hartinger, M., Rastaetter, L., & Sakharov, Y. (2023). Is the global MHD modeling of the magnetosphere adequate for GIC prediction: The May 27–28, 2017 storm. *Cosmic Research*, *61*(2), 120–132. https://doi.org/10.1134/s0010952522600044

Pulkkinen, A., Amm, O., & Viljanen, A., & BEAR Working Group. (2003). Ionospheric equivalent current distributions determined with the method of spherical elementary current systems. *Journal of Geophysical Research*, *108*(A2), 1053. https://doi.org/10.1029/2001JA005085

Pulkkinen, A., Bernabeu, E., Thomson, A., Viljanen, A., Pirjola, R., Boteler, D., et al. (2017). Geomagnetically induced currents: Science, engineering, and applications readiness. *Space Weather*, *15*(7), 828–856. https://doi.org/10.1002/2016SW001501

Pulkkinen, A., Rastatter, L., Kuznetsova, M., Singer, H., Balch, C., Weimer, D., et al. (2013). Community-wide validation of geospace model ground magnetic field perturbation predictions to support model transition to operations. *Space Weather*, *11*(6), 369–385. https://doi.org/10.1002/swe.20056

Pulkkinen, T. I., Brenner, A., Al Shidi, Q., & Toth, G. (2022). Statistics of geomagnetic storms: Global simulations perspective. *Frontiers in Astronomy and Space Sciences*, *9*. https://doi.org/10.3389/fspas.2022.972150

Reiter, K., Guillon, S., Connors, M., & Jackel, B. (2021). Statistics of large impulsive magnetic events in the auroral zone. *Journal of Space Weather and Space Climate*, *11*, 44. https://doi.org/10.1051/swsc/2021029

Russell, C. T., & McPherron, R. L. (1973). Semiannual variation of geomagnetic activity. *Journal of Geophysical Research*, *78*(1), 92–108. https://doi.org/10.1029/JA078i001p00092

Schillings, A., Palin, L., Opgenoorth, H. J., Hamrin, M., Rosenqvist, L., Gjerloev, J. W., et al. (2022). Distribution and occurrence frequency of dB/dt spikes during magnetic storms 1980–2020. *Space Weather*, *20*(5), e2021SW002953. https://doi.org/10.1029/2021SW002953

Tsurutani, B. T., Echer, E., Guarnieri, F. L., & Gonzalez, W. D. (2011). The properties of two solar wind high speed streams and related geomagnetic activity during the declining phase of solar cycle 2. *Journal of Atmospheric and Solar-Terrestrial Physics*, *73*(1), 164–177. https://doi.org/10.1016/j.jastp.2010.04.003

Tsurutani, B. T., & Gonzalez, W. D. (1987). The cause of high intensity long duration continuous AE activity (HILDCAAs): Interplanetary Alfven wave trains. *Planetary and Space Science*, *35*(4), 405–412. https://doi.org/10.1016/0032-0633(87)90097-3

Tsurutani, B. T., Gonzalez, W. D., Gonzalez, A. L. C., Guarnieri, F. L., Gopalswamy, N., Grande, M., et al. (2006). Corotating solar wind streams and recurrent geomagnetic activity: A review. *Journal of Geophysical Research*, *111*(A7), A07S01. https://doi.org/10.1029/2005JA011273

Tsurutani, B. T., Gonzalez, W. D., Gonzalez, A. L. C., Tang, F., Arballo, J. K., & Okada, M. (1995). Interplanetary origin of geomagnetic activity in the declining phase of the solar cycle. *Journal of Geophysical Research*, *100*(A11), 21733. https://doi.org/10.1029/95JA01476

Tsurutani, B. T., Gonzalez, W. D., Lakhina, G. S., & Alex, S. (2003). The extreme magnetic storm of 1–2 September 1859. *Journal of Geophysical Research*, *108*(A7), 1268. https://doi.org/10.1029/2002JA009504

Viljanen, A. (1997). The relation between geomagnetic variations and their time derivatives and implications for estimation of induction risks. *Geophysical Research Letters*, *24*(6), 631–634. https://doi.org/10.1029/97GL00538

Viljanen, A., Nevanlinna, H., Pajunpaa, K., & Pulkkinen, A. (2001). Time derivative of the horizontal geomagnetic field as an activity indicator. *Annales Geophysicae*, *19*(9), 1107–1118. https://doi.org/10.5194/angeo-19-1107-2001

Viljanen, A., Pirjola, R., Prácser, E., Ahmadzai, S., & Singh, V. (2013). Geomagnetically induced currents in Europe: Characteristics based on a local power grid model. *Space Weather*, *11*(10), 575–584. https://doi.org/10.1002/swe.20098

Viljanen, A., Tanskanen, E. I., & Pulkkinen, A. (2006). Relation between substorm characteristics and rapid temporal variations of the ground magnetic field. *Annales Geophysicae*, *24*(2), 725–733. https://doi.org/10.5194/angeo-24-725-2006

Weygand, J. M., Amm, O., Viljanen, A., Angelopoulos, V., Murr, D., Engebretson, M. J., et al. (2011). Application and validation of the spherical elementary currents systems technique for deriving ionospheric equivalent currents with the North American and Greenland ground magnetometer arrays. *Journal of Geophysical Research*, *116*(A3), A03305. https://doi.org/10.1029/2010JA06177

Weygand, J. M., Engebretson, M. J., Pilipenko, V. A., Steinmetz, E. S., Moldwin, M. B., Connors, M. G., et al. (2021). SECS analysis of nighttime magnetic perturbation events observed in Arctic Canada. *Journal of Geophysical Research: Space Physics*, *126*(11), e2021JA029839. https://doi.org/10.1029/2021JA029839

Woodroffe, J. R., Morley, S. K., Jordanova, V. K., Henderson, M. G., Cowee, M. M., & Gjerloev, J. (2016). The latitudinal variation of geoelectromagnetic disturbances during large ($Dst \leq -100$ nT) geomagnetic storms. *Space Weather*, *14*(9), 668–681. https://doi.org/10.1002/2016SW001376

Yermolaev, Y. I. (2023). Catalog of large-scale solar wind phenomena [Dataset]. Space Research Institute (IKI). http://www.iki.rssi.ru/pub/omni/catalog

Yermolaev, Y. I., Nikolaeva, N. S., Lodkina, I. G., & Yermolaev, M. Y. (2009). Catalog of large-scale solar wind phenomena during 1976–2000. *Cosmic Research*, *47*(2), 81–94. https://doi.org/10.1134/S0010952509020014

Zou, Y., Dowell, C., Ferdousi, B., Lyons, L. R., & Liu, J. (2022). Auroral drivers of large dB/dt during geomagnetic storms. *Space Weather*, *20*(11), e2022SW003121. https://doi.org/10.1029/2022SW003121